JSEE Vol. 25, No. 1&2, 2023 DOI: 10.48303/jsee.2023.1982829.1040

Research Paper

An innovative Multi-Level Energy Dissipative Device with a Combination of SMA Wire and Friction Damper

Mohammadghasem Vetr[1*] and Mehdi Saiidian[2]

1. Associate Professor, Structural Engineering Research Center, International Institute of Earthquake Engineering and Seismology (IIEES), Tehran, Iran,
*Corresponding Author; email: vetr@iiees.ac.ir
2. Ph.D. Candidate, International Institute of Earthquake Engineering and Seismology (IIEES), Tehran, Iran

Received: 14/12/2022
Revised: 24/10/2023
Accepted: 20/11/2023

ABSTRACT

Control systems' performance during earthquakes relies on reducing structural demand and absorbing seismic energy through an additive damping system. However, conventional dampers designed for design earthquakes may perform poorly during earthquakes below the DBE. To address this, multi-stage dampers have been developed to enable structures to perform acceptably at different seismic levels. This research project utilized a combination of friction damper and shape memory alloy to function in two phases. The proposed damper, FD-SMA, employs the SMA wire in the first phase and is combined parallelly with the friction part. The two-stage behavior results from a displacement gap that works in series with the friction damper. One significant benefit of the proposed damper is that the first fuse remains undamaged during moderate earthquakes due to the shape memory alloy's superelasticity. This leads to maintaining the structure's performance in future earthquakes without needing repairs. Additionally, the residual displacement is expected to decrease in both stages. A small-scale model of the proposed damper was fabricated and evaluated in the structural laboratory of IIEES. The behavior was also modeled in OpenSees. In all experimental tests, the desired dual-stage performance was achieved. As anticipated, using SMA reduced residual displacement and minimized damage in the first stage due to its recentering property. The first fuse shows acceptable elasticity and remains undamaged when excluding unwanted friction.

Keywords:
Hybrid passive damper;
Two-phase system;
Shape memory alloy;
Friction damper

1. Introduction

Earthquakes can cause significant damage to structures, both structurally and non-structurally, due to the high amount of energy they generate. Traditional systems are designed with stiffness, strength, and flexibility in mind to withstand earthquakes, but this approach may need to be more cost-effective and efficient for unforeseen seismic events (Hongnan & Huo, 2010) (Song, et al. 2006). Over the past few years, researchers have studied ways to control structural vibrations and safeguard lives and property from earthquake risks. They've devised two innovative systems: seismic isolation and energy dissipation. Seismic isolation systems work by minimizing the energy that passes into the structure (Christopoulos & Filiatrault, 2006). Passive energy dissipation systems are created to reduce harm to critical structural elements by directing the plastic deformation to controlled locations within building structures and absorbing seismic energy. This can help to decrease the demand for energy dissipation. Passive systems that utilize devices are particularly

beneficial due to their low cost and minimal maintenance needs. A variety of passive dampers have been used in buildings (Soong & Spencer, 2002) (Symans, et al., 2008). The characteristics of dampers in a passive energy-dissipating system are determined to reduce structural response during a design earthquake. However, these dampers may be damaged during moderate earthquakes, causing their performance to decrease during the main shock. In contrast, conventional passive dampers perform poorly during moderate earthquakes. To address this issue, auxiliary fuses can reduce structural seismic responses during moderate earthquakes without engaging the main fuse.

Recent studies have focused on hybrid dampers, which offer a more cost-efficient and optimized approach to controlling vibration levels. These dampers can dissipate energy effectively at different seismic levels by combining multiple control systems with varying strength and stiffness. They also offer the benefits of other dampers in one device. However, passive dampers can increase stiffness in the primary structure, which may elevate specific responses, such as acceleration or velocity. Moderate earthquakes demand lower deformation demands on structures, and excessive input energy can result from the unnecessarily high global stiffness of the structure.

1.1. SMA (Shape Memory Alloy)

A significant focus has been on creating a new method for managing earthquake-induced residual drifts and structure story control. This has resulted in numerous studies investigating the potential of using shape memory alloys (SMA) as an innovative material for dynamic damping structures. SMAs are a new material type with unique characteristics, such as shape memory effect (SME), superelasticity effect (SE), exceptional fatigue resistance, high corrosion resistance, high damping traits, and temperature-dependent Young's modulus. These properties make them suitable for seismic applications, such as their ability to endure high fatigue and exhibit superelasticity (Duerig, et al., 1990) (Dolce & Cardone, 2001). SMA-based dampers can resist significant strains without any deformation remaining after unloading. This is due to their superelasticity, which allows them to absorb energy during cyclic loading. Compared to dampers made of other metallic materials, SMAs have superior properties because of their martensitic phase transformation, which can be triggered by either temperature or stress. SMAs are two-phase metals that can exist in either austenitic or martensitic form (Lagoudas, 2008).

SMAs have two mechanical properties depending on the temperature of the material. If the temperature is high, they exhibit the *SE*, where strains from loading are fully recovered after unloading (known as superelasticity). If the temperature is low, they show the SME, where residual stresses remain after unloading but can be recovered by heating above the austenite finish temperature (Lagoudas, 2008). This property is called a shape memory effect, as shown in Figure (1).

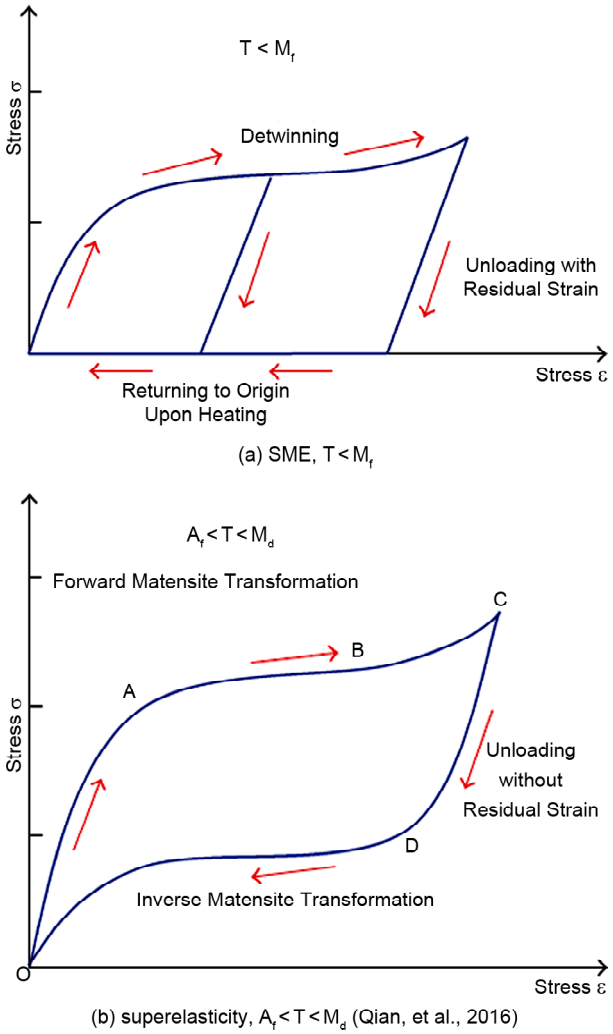

Figure 1. Stress-Strain diagrams of N_iT_i shape memory alloy.

1.2. Two-Stage Damper

Passive dampers are designed to minimize structural response during a design earthquake. However, multiphase energy-dissipating devices may sustain damage in moderate earthquakes, reducing efficiency during the mainshock. To address this issue, two-phase control systems have emerged. These systems comprise auxiliary fuses for moderate earthquakes and a main fuse for the design earthquake. The first fuse operates independently during moderate earthquakes, leaving the main fuse intact for the design earthquake. Passive dampers can reduce specific structural responses like story drift. However, they also increase the structure's stiffness, which can lead to higher acceleration or velocity. During moderate earthquakes, structures endure lower deformation demands than during designed earthquakes. Thus, increasing the global stiffness of a building during a moderate earthquake can cause an unwanted increase in input energy. Using two-phase dampers makes designing structures for two seismic levels possible, ensuring predictable and controlled behavior during earthquakes. Unlike conventional dampers, which can only be designed for designing earthquakes, two-phase dampers increase the degree of freedom and redundancy of structures, improving their reliability. These devices can also enhance the system's R-factor, ductility, and hysteresis damping while absorbing energy faster. However, conventional dampers may not respond predictably to moderate shocks.

1.3. Friction Damper

Friction dampers have numerous advantages, including easy manufacturing and installation, reasonable pricing, stable damping behavior, high damping, velocity, and temperature independence. Among the various models of friction dampers proposed in previous research, the Slotted Bolted Connection damper has been selected for this study. This damper requires a friction pad made using brake pads due to its high friction coefficient, stable performance, and ability to withstand numerous loadings without damage. A new and innovative idea for a two-stage damper using shape memory alloys and friction devices aims to combine the benefits of both systems.

2. Past studies

Qiu and Zhu (2017) introduced a bidirectional SMA damper that was tested on a seismic table. The results showed that the damper did not require any repairs or replacements even after multiple experiments, indicating its ability to withstand earthquakes without sustaining damage. Other studies, such as those conducted by Morais et al. (2017) and Qian et al. (2013), have also observed the need to stretch the wire in both directions. Although SMA was found to have recentering abilities in the austenite phase, it lacked significant energy dissipation during this phase. To address these shortcomings, subsequent studies proposed using hybrid dampers that incorporate SMA wire to enhance the behavior of SMA dampers.

The study by Yang et al. (2010) demonstrates the effectiveness of a hybrid SMA damper that utilizes an energy-absorbing strut to achieve high recentering and energy absorption capacity. Qian et al. (2016) study found that the friction can increase energy absorption, significantly reducing displacement, drift, and acceleration in stories.

Ozbulut and Hurlebaus (2012) developed a hybrid damper for a 20-story building with a friction pad and SMA wire. They found that this damper effectively reduced the relative displacement of stories by up to 55% and the maximum story acceleration by up to 43%. Additionally, residual story drift was noticeably reduced. Other researchers, such as Li et al. (2008), utilized friction pads in their suggested model, Wang et al. (2013) used viscous dampers, and Karavasilis et al. (2011) used a viscoelastic core surrounded by SMA wire.

Marshal and Charney (2010) suggest adding high-damping materials in series with buckling resisting braces during two different response phases (Rawlinson & Marshal, 2012).

Several researchers have proposed various hybrid systems that utilize yielding and frictional dampers to control the impact of earthquakes on steel structures. These systems come in different forms, such as the Yielding Pipe and frictional damper combination suggested by Beheshti-Aval et al. (2013). Yamamoto and Sone (2014) proposed a two-stage system that uses yielding and viscoelastic dampers. Hashemi and Moaddab (2017) introduced two hybrid dampers that combine

different friction and yielding dampers to achieve two performance levels. Zahrai and Golmoghany (2021) introduced a new hybrid control system that comprises a Friction Damper and a Vertical Shear Panel (HFD-VSP) in series. The proposed system utilizing FD and VSP performs better than the vertical shear panel against a wide range of earthquakes, including the mainshock with strong foreshocks and aftershocks. Cheraghi and Zahrai (2016) developed a multi-level Yielding Pipe Damper that utilizes concentric circles to control the structure's response to various earthquake intensities. Li et al. (2019) recommended combining conventional BRBs with metal tube dampers to create a novel two-level damper. The tube damper yields under frequent earthquakes to consume seismic energy, and the core plate yields under rare earthquakes to further dissipate energy and reduce the seismic effect. Golmoghany and Zahrai (2021) proposed a double-vertical Shear Panel, D-VSP, to improve structures' seismic behavior, combining two vertical shear panels in series in a chevron bracing configuration. D-VSP is expected to beneficially change dynamic behavior parameters like strength, stiffness and damping ratio through increasing ductility by utilizing two levels of energy for two different earthquake intensity levels. Rousta and Zahrai (2017) introduced a novel two-level control system to enhance chevron-braced steel frames' performance. By integrating two Knee Braces (KB) and a Vertical Link Beam (VLB) into a chevron-braced frame, this system can effectively withstand both main shock and aftershocks in steel structures. Cheraghi and Zahrai (2019) present practical manufacturing details for a new multi-stage damper with nested pipes capable of changing dynamic behavior parameters, including strength, stiffness and damping ratio.

3. Research Objectives

The research aims can be summarized as follows:

- To prevent damage and entry into the nonlinear phase of the main fuse in earthquakes below the DBE, the auxiliary fuse should absorb energy during moderate earthquakes while keeping the main fuse undamaged.
- To use the shape memory alloy to recenter and minimize permanent displacement in the first level of earthquake while reducing it in the second level.
- To design two earthquake levels with two-phase performance ensures that the structure can withstand moderate and severe earthquakes. However, current dampers are only meant for design earthquakes, which means they may not be effective in moderate earthquakes that are more common.
- To use a shaped memory alloy in the initial fuse reduces damage during moderate earthquakes and maintains performance for future ones.
- To provide a passive control system with higher reliability than other passive controllers using a two-stage fuse formation.
- Systems with two fuses start the energy absorption earlier in moderate earthquakes than single-stage systems.

4. This Paper

This paper focused on combining shape memory alloy dampers and friction dampers to meet the damping requirements of two different levels of seismic demands. The proposed method incorporated these dampers to utilize the SMA wire as an auxiliary fuse to absorb energy during moderate seismic activity and protect the structure without affecting the main fuse. However, due to the low damping capacity of the SMA wire, a friction damper was added to enhance the absorption capacity during severe seismic activity. The study used NATIONAL alloy and explored the superelasticity property at room temperature.

The performance of a Friction Damper can be affected by different factors, including surface finish, sliding velocity, normal force, contact pressure, wear and temperature (Blau, 2009). Lee et al. (2016) suggested using an automotive braking pad as the friction pad for a friction damper to achieve reliable performance and high energy absorption. This design is less sensitive to loading amplitude, frequency, velocity, and ambient temperature.

The hybrid damper (FD-SMA) consists of a shear-type friction damper and an SMA damper to effectively dissipate seismic energy. The SMA

damper dissipates energy during low-to-moderate demand levels and can create stable, uniform, and recentering hysteresis. During a strong earthquake, the Friction damper works simultaneously with the SMA wire to continuously dissipate energy through friction. Limiting the operating range of different dampers according to the seismic demand can minimize repair and replacement costs, ultimately saving life cycle costs. The SMA wires have unique features such as recentering ability, which can reduce residual deformation and device destruction, contributing significantly to the FD-SMA performance.

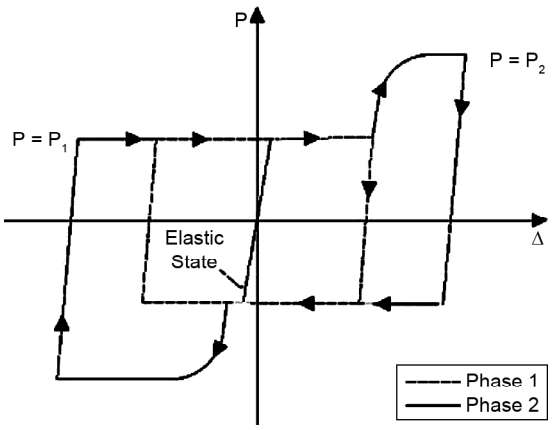

Figure 2. Ideal hysteresis curve for a two-level system.

4.1. The Geometry of |Two-Stage Dampers

This study explores a proposed composite damper made of a parallel combination of memory alloy and friction damper. The damper consists of two parallel springs with a gap displacement, which creates main and auxiliary fuses. The SMA wires act as the first fuses, and the friction dampers act as primary fuses. After exceeding a predetermined gap spacing, the SMA wires and friction dampers work together in parallel to absorb energy. In medium-magnitude earthquakes, absorbing energy in the auxiliary fuse is possible without engaging the main fuse.

The energy absorption system can demonstrate a two-phase behavior through a displacement gap. An additional fuse is added to the system to absorb more energy as the intensity of an earthquake and the damper displacement increase. Two dampers are made for medium and severe earthquake levels, each with separate strength and stiffness requirements. Figure (2) shows the ideal hysteresis curve for a two-stage damper under cyclic loading. The energy absorption system depends on displacement in both phases.

When the P force increases beyond the maximum allowable force in the first phase, sliding occurs between the plates in the auxiliary fuse. The yielding of SMA wires initiates this sliding. If the maximum displacement continues in the same direction, the sliding between the plates will continue. At this point, the hybrid behavior is activated by using both phase 1 and phase 2 over several stages. If the displacement exceeds the maximum displacement range of the specified slip range, then the second level of the damper comes into operation. The device goes into phase 2, and friction is used to join the energy absorption procedure.

During this stage, the energy is dissipated through the second damper's friction and the first damper's superelastic behavior. This results in a significant increase in the utilization of energy dissipation compared to phase 1. To prevent excessive deformation in a particular direction, it is essential to increase the load resistance capacity in phase 2, particularly when the dampers are exposed to different levels of cyclic loads during an earthquake.

The basic requirements for hybrid dampers in multi-stage behavior can be summarized as follows:

a) Dampers should be designed to dissipate lateral force energy during earthquakes without being activated by wind lateral force.
b) A suitable damper range should be predicted based on permitted displacement to prevent excessive deformation.
c) The values of P1 and P2 should be determined based on the required earthquake level demand.
d) The supports must possess sufficient strength to endure the anticipated maximum force.

Figure (3) illustrates the FD-SMA damper design. The top plate is connected to one end of the bracket, while the bottom is connected to the other. The plates can slide over each other through slots. The device's intended gap produces a two-level displacement-dependent performance.

This mechanism works in two stages. When there is a lateral displacement, it is first transmitted

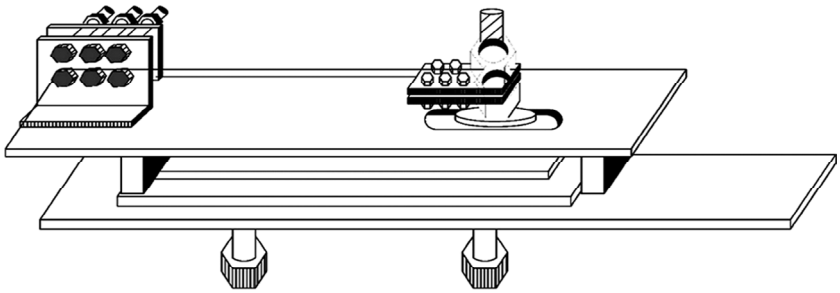

Figure 3. FD-SMA damper geometry.

through the SMA wires in the first stage of the damper. Once the displacement increases and reaches the end of the horizontal gap, the friction plate comes into play and enters the second phase.

4.2. Two Stage FD-SMA Damper

Equations (1) to (4) present the general equations for modeling the two-stage effect of fuse stiffness.

$$F_s = k_{d1}u \tag{1}$$

$$F_s = \alpha.K_{d1}\left(u - \Delta_{yd1}\right) + f_{y1} \tag{2}$$

$$F_s = \alpha.K_{d1}\left(u - \Delta_{yd1}\right) + f_{y1} + k_{d2}\left(u - \Delta_{gap}\right) \tag{3}$$

$$F_s = \alpha.K_{d1}\left(u - \Delta_{yd1}\right) + f_{y1} + f_{y2} + \alpha.K_{d2}\left(u - \Delta_{yd2}\right) \tag{4}$$

In the given equations, K_{d1} and K_{d2} represent the elastic stiffness of the first and second fuses, respectively. The force-displacement relationship is linear till the yielding displacement of the first fuse, which Δ_{yd1} describes. In this step, only the first fuse is sufficient. After increasing the displacement to more than the displacement of the first fuse, a stiffness value of $\alpha.K_{d1}$ is added to the displacement force relation in Equation (2). As the displacement increases, and the displacement is less than the yield displacement of the second fuse, the elastic force of the second fuse, K_{d2} $(u - \Delta_{gap})$, is cumulatively coupled to the final force of the first fuse $(\alpha.K_{d1}(u - \Delta_{yd1}) + f_{y1})$, as shown in Equation (3). Finally, after increasing the displacement to more than the yield displacement of the second fuse (Δ_{yd2}), the effects of strain hardening of the second fuse are also cumulatively added to the sum of forces $(\alpha.K_{d2}(u - \Delta y_{d2}))$, as shown in Equation (4).

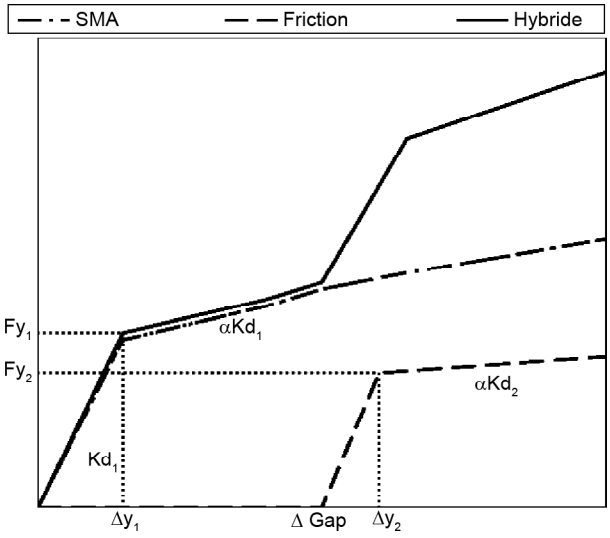

Figure 4. Multilinear force and displacement curves for FD-SMA hybrid dampers.

Figure (4) illustrates the relationships presented and demonstrates the effect of each fuse segment on the FD-SMA damper.

5. The Geometry of FD-SMA Dampers

Dampers typically have three main components. The bottom plate supports the brake pad, while the middle plate creates friction with the brake pad. The upper part is where SMA wires are assembled. The top two sheets of the damper contain slotted holes that allow the sheets to move and slide easily.

Dampers are composed of three main components. The bottom plate serves as the brake pad support, the middle plate provides friction with the brake pad, and the upper part is where SMA wires are assembled. The top two sheets have slotted holes to enable them to move and slide smoothly (Figures 5 to 7).

Figure (8) shows a complete assembly of the FD-SMA damper (Figures 9).

The dampers' plan and section are detailed in Figures (10) , (11) and (12).

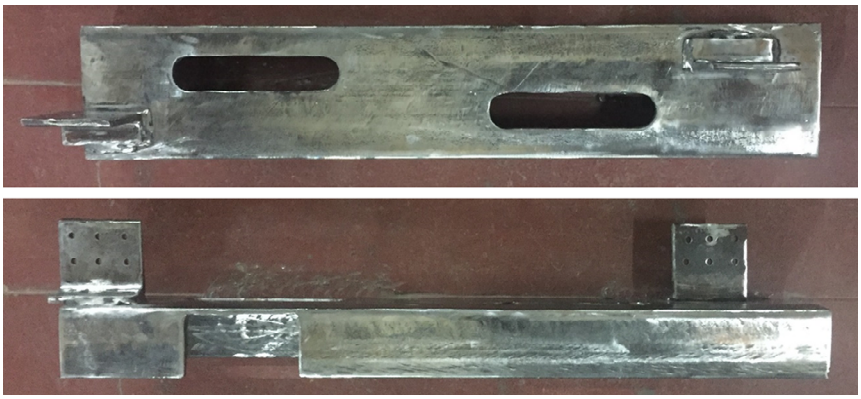

Figure 5. Multilinear force and displacement curves for FD-SMA hybrid dampers.

Figure 6. The lower plate of the FD-SMA damper with asbestos 10 mm brake pad.

Figure 7. The middle plate of the FD-SMA damper.

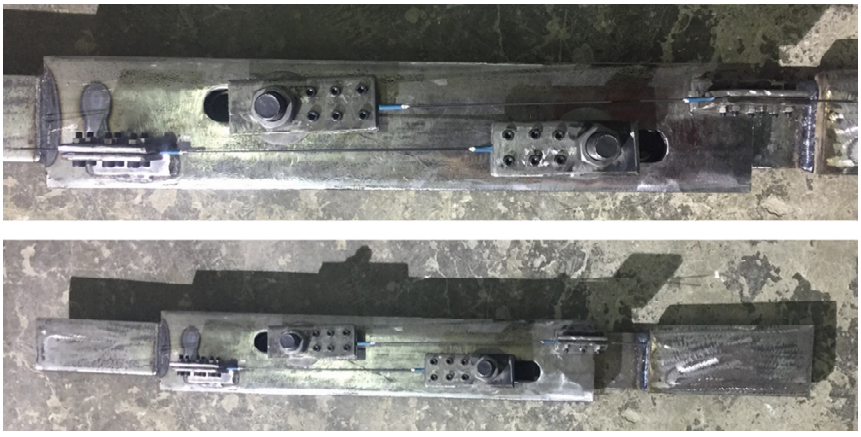

Figure 8. Assembled FD-SMA damper (top).

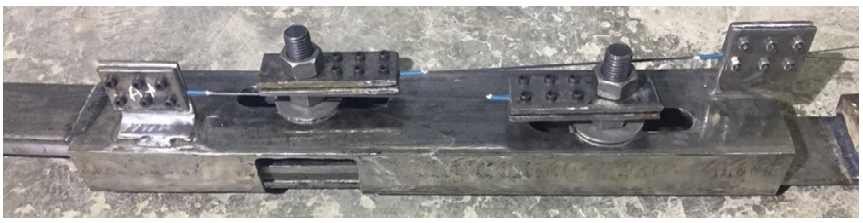

Figure 9. Assembled FD-SMA damper (side).

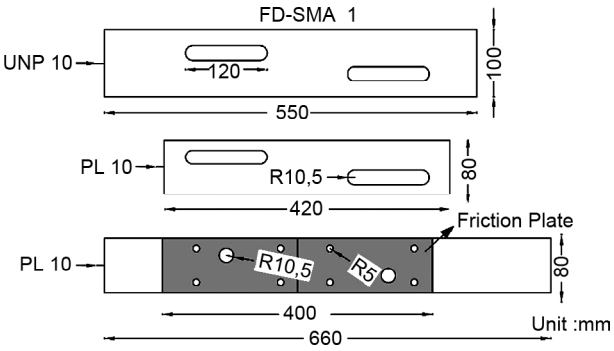

Figure 10. FD-SMA damper plan.

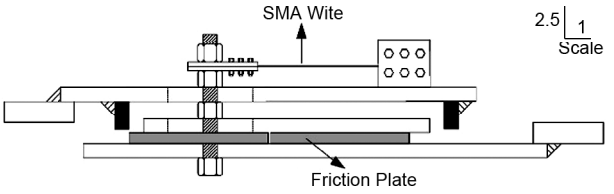

Figure 11. FD-SMA damper section.

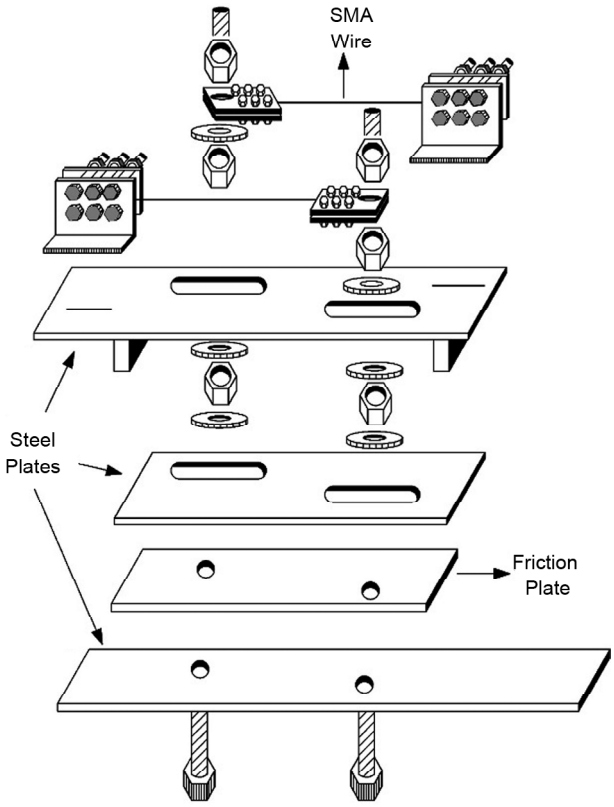

Figure 12. Assemble procedure of FD-SMA damper.

6. Experimental Studies

Experimental studies were conducted on a small-scale sample to assess the proposed dampers' performance accurately. The damper consists of two separate components that function as a two-stage damper. The experiments conducted on the model were divided into three stages, which included testing the friction part of the damper, the SMA wire part separately, and the simultaneous performance testing of these two parts as a two-stage damper. These experiments were carried out at the International Institute of Seismology and Earthquake Engineering (IIEES) laboratory using the Roell Amsler Model REL 2191. The sinusoidal cyclic displacement controlled loading was performed within specified domains. The universal testing machine also examined the dynamic behavior of the 1 mm diameter wire of the shape memory alloy used in the fabrication of the damper. The time-displacement diagram applied to the SMA wire is shown in Figure (13). The range of the jaw cycle is from 1 mm until the wire ruptures at 38 mm, with 1 mm steps and five cycles per step. Figure (14) shows the force-displacement diagram of the SMA wire. The diagram indicates that the strain hardness phase begins at a displacement above 20 mm (10% strain).

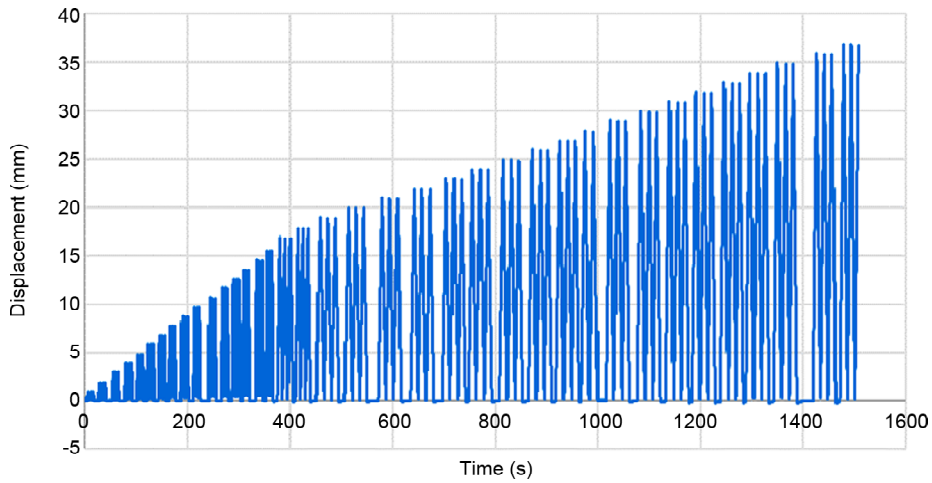

Figure 13. SMA wire displacement cycles.

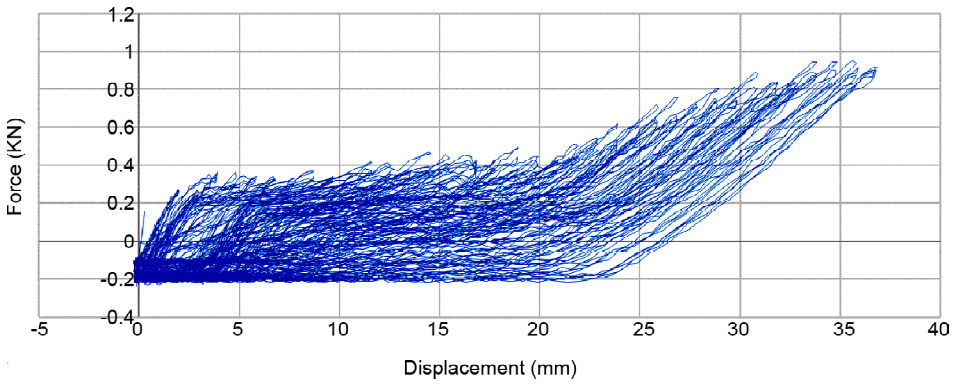

Figure 14. SMA wire force-displacement diagram.

The hysteresis behavior of the FD-SMA damper was studied by subjecting it to sine loading cycles using a universal testing machine, as shown in Figure (15).

Figure (16) shows the positioning of the FD-SMA damper on a universal machine ready for testing.

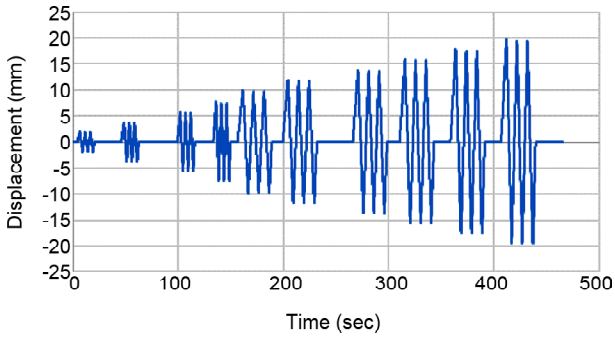

Figure 15. Time-displacement diagram applied to the FD-SMA dampers.

7. Experimental Results and Observations

The FD-SMA damper was tested by loading its components separately to examine the friction, SMA and combination parts. The test results are presented in the form of a force-displacement graph. In addition to the cyclic behavior of the damper, the study of friction dampers also considers obtaining the optimum slip force for the hybrid device. Figure (17) displays the force-displacement diagram of the frictional section of the FD-SMA damper with varying screw prestress.

The FD-SMA damper force-displacement diagram is shown in Figure (18).

A diagram depicting the behavior of the FD-SMA damper is presented in Figure (19). The dampers exhibit a multi-linear pattern in their response. In the tensile phase, the initial stiffness of the dampers is 1.42, which gradually decreases

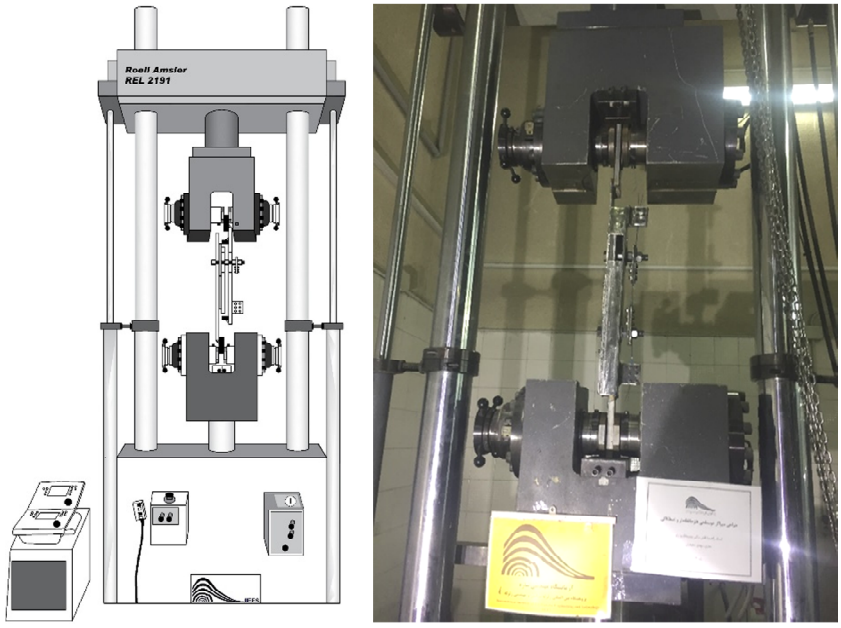

Figure 16. Installation of FD-SMA dampers in the universal machine.

to a secondary stiffness of 0.125 kN/mm. In the second phase, the initial hardness 0.0989 is reduced to a secondary hardness of 0.074.

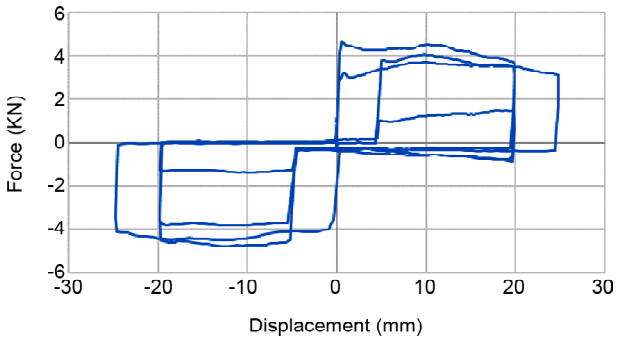

Figure 17. Force-displacement diagram of the frictional part of the FD-SMA damper.

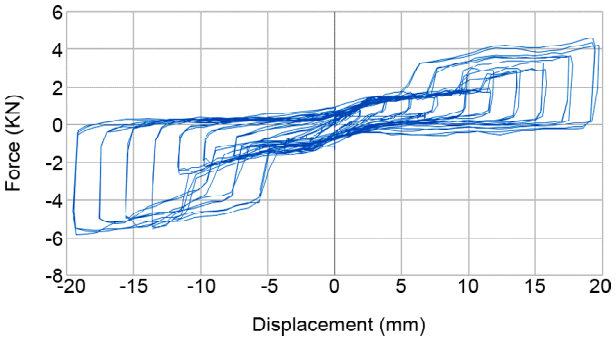

Figure 18. FD-SMA dampers force-displacement diagram.

Notably, the stiffness during the tensile and compression phases is roughly similar.

Some parameters obtained from the experiment are shown in Table (1).

Table (2) shows some of the properties of the FD-SMA damper.

Based on Figure (20), the model has demonstrated an increase in energy absorption during the second phase of the damper. Additionally, Figure (21) shows that the average equivalent viscous damping of its cycles is 20%, with a minimum of 15%.

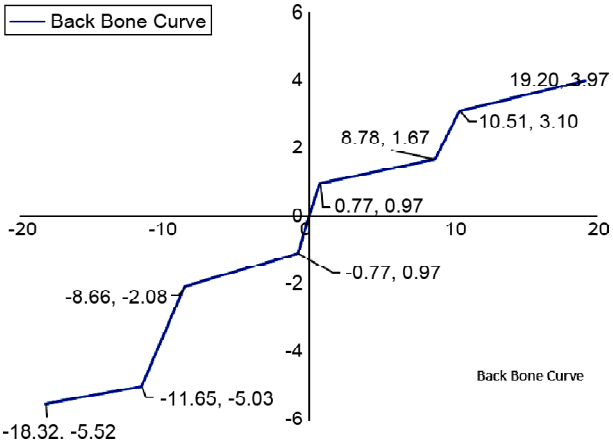

Figure 19. Idealized multi-linear diagram of FD-SMA damper.

Table 1. Some parameters of FD-SMA damper obtained from the experiment.

Positive Part		Yielding Force, Py (KN)	0.972
		Maximum Force, Pmax (KN)	3.972
	First Fuse	Initial Stiffness Kd_1 (KN/mm)	1.422
		Secondary Stiffness Kd'_1 (KN/mm)	0.125
	Second Fuse	Initial Stiffness Kd2 (KN/mm)	0.989
		Secondary Stiffness Kd'_2 (KN/mm)	0.074
Negative Part		Yielding Force, Py (KN)	1.091
		Maximum Force, Pmax (KN)	5.523
	First Fuse	Initial Stiffness Kd_1 (KN/mm)	1.267
		Secondary Stiffness Kd'_1 (KN/mm)	0.087
	Second Fuse	Initial Stiffness Kd_2 (KN/mm)	0.826
		Secondary Stiffness Kd'_2 (KN/mm)	0.100

Table 2. Some of the properties of the FD-SMA damper.

Cycle #	2	4	6	8	10	12	14	16	18	20
Area Bellow Curve	1.65	6.13	11.20	17.76	27.21	37.78	55.39	66.33	100.72	145.02
Max x	1.86	3.87	5.81	7.69	9.894	11.86	13.86	15.80	17.79	19.75
Min x	-1.89	-3.74	-5.64	-7.52	-9.8	-11.73	-13.65	-15.62	-17.57	-19.50
Max F	0.88	1.54	1.78	1.57	2.642	2.96	2.96	3.34	3.65	4.60
Min F	-1.38	-1.59	-1.58	-1.83	-2.2	-2.66	-5.52	-5.43	-5.26	-5.81
K_{eff}	0.60	0.41	0.29	0.22	0.25	0.24	0.31	0.28	0.25	0.27
Δ_{avg}	1.88	3.80	5.72	7.60	9.85	11.79	13.76	15.71	17.68	19.62
β_{eff}	0.12	0.16	0.19	0.22	0.18	0.18	0.15	0.15	0.20	0.23

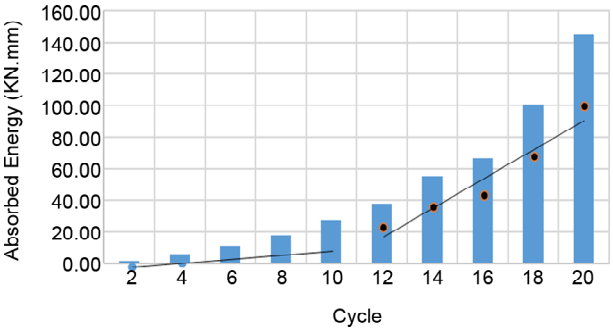

Figure 20. Absorbed energy per each cycle of FD-SMA damper.

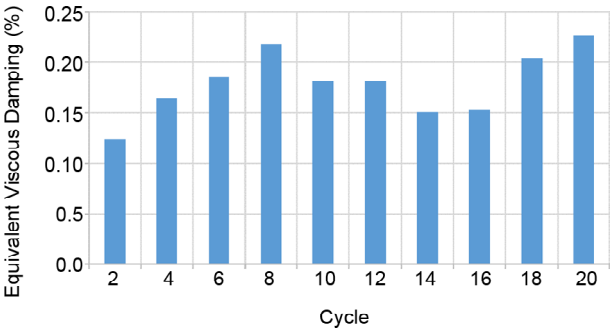

Figure 21. Equivalent viscous damping diagram for each cycle in the FD-SMA damper.

8. Numerical Modeling

To accurately assess the performance of the proposed damper, the FD-SMA damper was also examined numerically using OpenSees software. The modeling aimed to validate and match the cyclic behavior obtained in the test with their analytical behavior to perform a simple parametric comparison. Each part of the FD-SMA damper was validated separately, and finally, the hybrid two-stage FD-SMA damper was modeled by combining the behavior of these two parts.

There are various reasons why the data stored by the universal device can fluctuate, such as environmental vibrations, non-ideal equipment and test conditions. These fluctuations lead to a not-so-smooth graph. To eliminate these fluctuations, different filters can be used. This research used a moving average filter to smooth the curve. This filter acts as an operator and can select the desired frequencies from a range to obtain a non-random time series.

In OpenSees (2006), the behavior of the proposed damper is modeled using uniaxial material elements. The simplified FD-SMA damper model comprises three components that are combined. The friction dampers and displacement gaps work in series, parallel to the SMA wire part. All forces enter the SMA wire before exceeding the gap displacement, and after exceeding the gap displacement, the friction damper combines in parallel with the SMA wire (Figure 22).

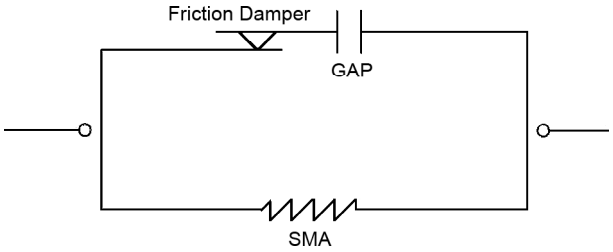

Figure 22. Schematic modeling of the FD-SMA damper.

The analytical behavior of the SMA wire and the experimental diagram are compared in the first step. Since the wire is not fully stretched at the beginning of the test, the first few millimeters of the SMA wire diagram are not stretched and are almost horizontal, so this section needs to be included. It was observed that they differ by only about 2.24% in area, which is a perfectly acceptable match (Figure 23).

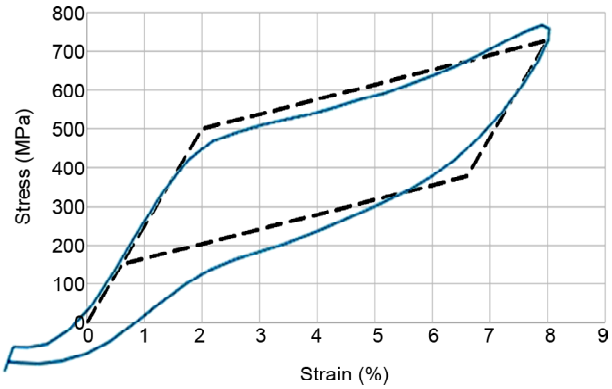

Figure 23. Matching experimental and analytical diagrams of SMA wire.

There are some reasons why the behavior of the SMA damper part differs from that of the SMA wire alone. The primary reason is the friction of the damper's top plate, which partially affects the test results due to the low test forces used. The area of the two curves was calculated, and it was found that the size below the curves differs by approximately 7.57%, which is an acceptable margin for matching experimental and numerical curves (Figure 24).

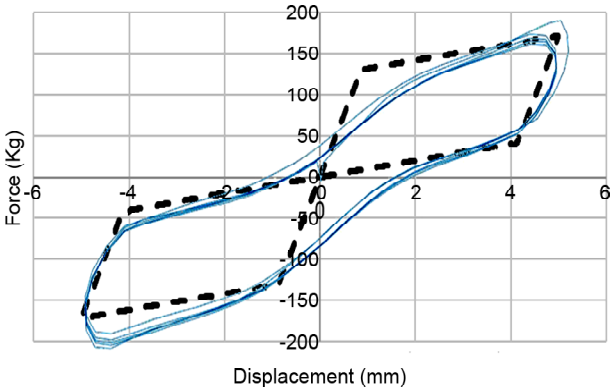

Figure 24. Matching experimental and analytical diagrams of the SMA part of the FD-SMA damper.

The absorbed energy of the experimental output of the friction part differs by 27.53% from the analytical output. Although the slope of the curves is precisely matched, the difference in the area can be attributed to the friction and shocks generated in the laboratory sample (Figure 25).

A comparison of numerical and experimental results on the FD-SMA damper parameters, including maximum displacement, maximum force, equivalent stiffness, damping, and energy absorption, over five different cycles is presented in Table (3) and Figure (26).

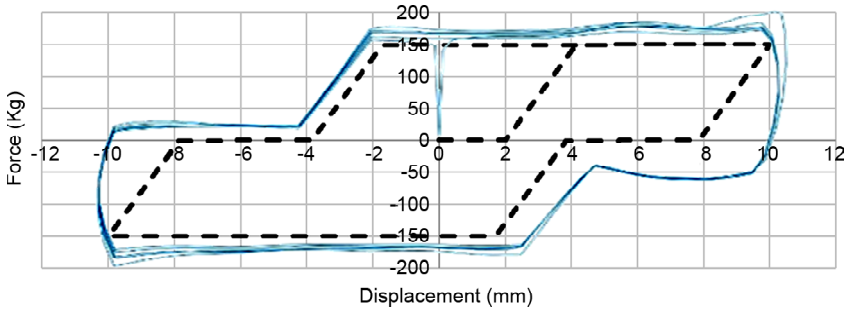

Figure 25. Matching experimental and analytical diagrams of friction and gap part of the FD-SMA damper.

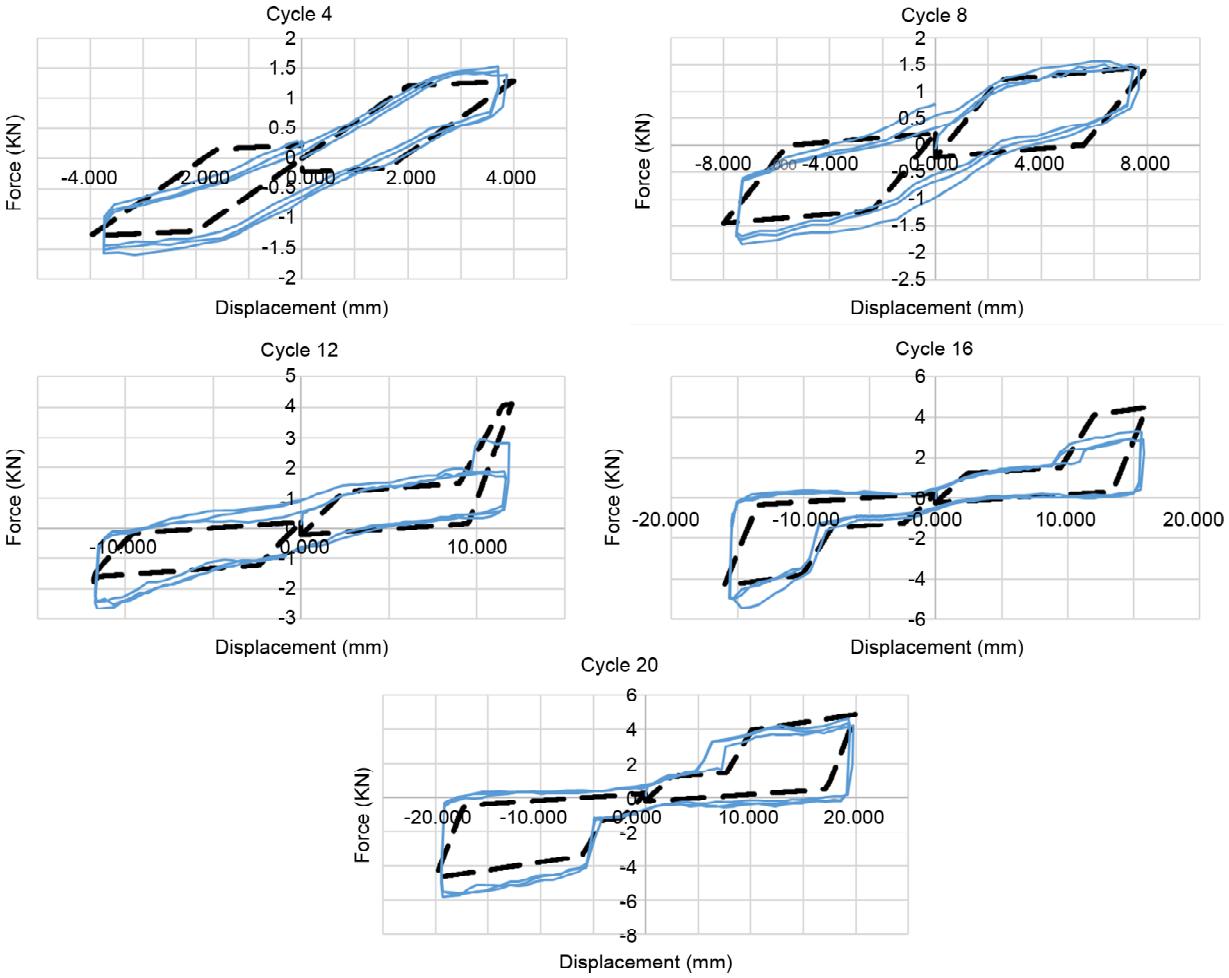

Figure 26. Matching experimental and analytical diagrams of FD-SMA damper.

Table 3. Experimental and analytical parameters of FD-SMA damper.

	(Exp-Num)/Exp%					
Cycle#	**4**	**8**	**12**	**15**	**20**	**Average**
A	13.7.565	15.28029	28.56685	9.391127	27.96821	18.98842
Max x	5.152471	5.200868	1.755279	1.832994	1.913425	3.171007
Max F	17.82214	14.74669	35.86317	2.300639	6.865629	15.51965
K_{eff}	21.84885	18.9614	36.96954	0.459227	8.614226	17.37065
β_{eff}	0.170933	5.538702	9.454953	13.02311	24.1103	10.4596

9. Parametric Studies of FD-SMA Damper

The damper's primary behavior in each phase depends on a specific parameter. The SMA wire's yield force, which depends on its cross-section area, is the effective parameter in the first level. In the second level, the sliding force of the friction damper is the controller. The ratio of the SMA wire yield force to the friction part's slip force is denoted as (λ). There are 15 models of λ, ranging from 0.1 to 1.5, with steps of 0.1. The amount of energy absorbed, and equivalent damping is used to compare the behavior of dampers. It was observed that as λ increases, energy absorption increases.

However, the increase is not significant after $\lambda = 11$. Additionally, the equivalent damping does not increase significantly after $\lambda = 9$.

Normalized absorbed energy and equivalent damping are plotted on a single graph to examine them together.

The diagram shows that a cross-sectional area of 3 mm^2, equal to $\lambda = 10$, exhibits the optimal behavior of this small-scale damper. However, increasing λ leads to a slight increase in energy absorption and equivalent damping. It is important to note that a further rise in cross-section is not recommended due to economic issues and the high cost of SMA wire.

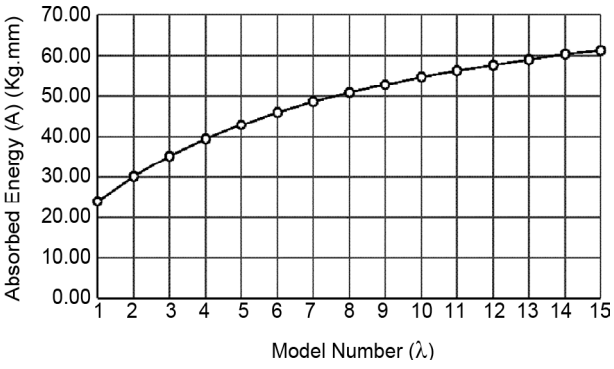

Figure 27. Graph of absorbed energy for FD-SMA dampers with different λ.

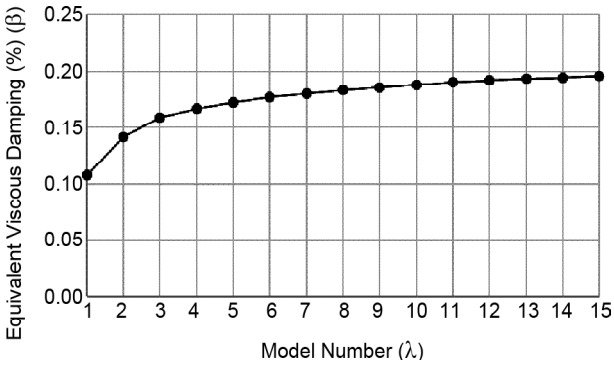

Figure 28. Graph of equivalent viscous damping for FD-SMA dampers with different λ.

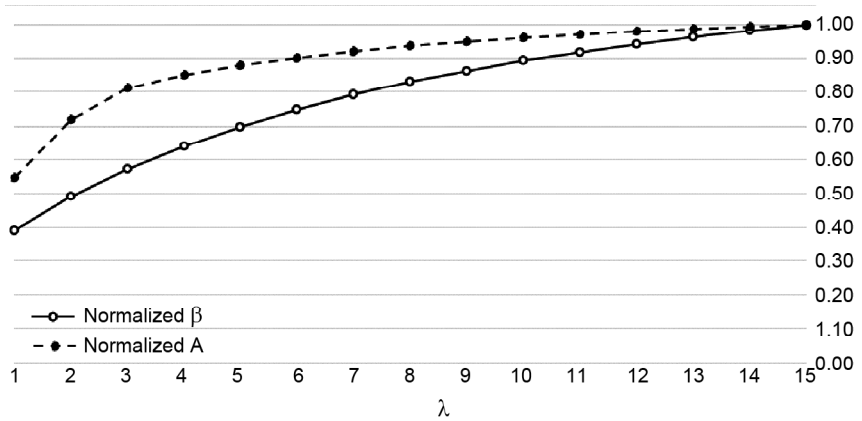

Figure 29. Comparison of equivalent damping and energy absorption of models with different λ.

10. Conclusion

All the laboratory samples have successfully achieved a two-level performance of the dampers. The first fuse enters a nonlinear performance before the gap displacement, during which the main fuse does not join in the behavior. However, as the displacement increases and surpasses the gap displacement, the main fuse gets involved in the behavior and improves the damping.

The shape memory alloy's recentering property may be affected, but the damper can significantly reduce permanent displacement in its first and second stages.

Upon analysis of the equivalent viscous damping of the samples, it was found that the average damping was at 20%. However, it is feasible to attain greater damping by adjusting the ratio of damping parameters at the first and second levels, such as wire diameter and the compressive force of friction plates.

Based on the diagrams, it is evident that the absorbed energy is considerably low before reaching the displacement gap. However, upon reaching the displacement gap and the subsequent engagement of the second fuse, there is a significant increase in the sample's energy absorption, demonstrated by a steep slope.

Based on the displacement force curves obtained from FD-SMA composite dampers, it has been observed that the first phase diagram related to SMA wires has been affected by unwanted friction between the plates. However, it should be noted that the unwanted friction is significant only when compared to the force generated in the wires due to the small scale of the sample. This error can be ignored if the model is manufactured and tested on a large scale. Failure to consider the impact of unwanted friction results in recentering behavior that is not ideal in the first phase. Therefore, the proposed damper aims to prevent damage to the main fuse in moderate earthquakes while minimizing damage to the secondary fuse.

The comparison between the OpenSees finite element model and the laboratory model shows that they behave similarly. The average energy absorption was around 82%, the maximum force generated in each cycle was around 85%, and the equivalent viscous damping of the cycles was around 90%. Overall, the results indicate a good agreement between the two models.

After parametric studies on various damper models with different characteristics, it was found that the damper with an SMA wire yielding force equal to the friction plate slip force exhibited superior behavior.

References

Beheshti-Aval, S.B., Mahbanouei, H., & Zareian, F. (2013). A hybrid friction-yielding damper to equip concentrically braced steel frames. *International Journal of Steel Structures*, *13*(4), 577-587.

Blau, P.J. (2009). *Friction Science and Technology: from Concepts to Applications (2nd ed.)*. Boca Raton, FL (USA): CRC Press.

Cheraghi, A., & Zahrai, S.M. (2016). Innovative multi-level control with concentric pipes along brace to reduce seismic response of steel frames. *Journal of Constructional Steel Research*, *127*, 120-135.

Cheraghi, A., & Zahrai, S.M. (2019). Cyclic testing of multilevel pipe in pipe damper. *Journal of Earthquake Engineering*, *23*(10), 1695-1718.

Christopoulos, C., & Filiatrault, A. (2006). *Principles of Passive Supplemental Damping and Seismic Isolation*. Pavia (Italy): IUSS Press.

Dolce, M., & Cardone, D. (2001). Mechanical behavior of shape memory alloys for seismic applications. *International Journal of Mechanical Sciences*.

Duerig, T.W., Melton, K.N., Stockel, D., Wayman, & M.C. (1990). *Engineering Aspects of Shape Memory Alloys*. London, UK: Butterworth Heinemann.

Golmoghany, M.Z., & Zahrai, S.M. (2021). Improving seismic behavior using a hybrid control system of friction damper and vertical shear panel in series. *Structures*, *31*, 369-379.

Hongnan, L., & Huo, L. (2010). Advances in structural control in civil engineering in China. *Mathematical Problems in Engineering*, *2010*(2), Article ID936081. doi:10.1155/2010/936081

Hosseini Hashemi, B., & Moaddab, E. (2017). Experimental study of a hybrid structural damper for multi-seismic levels. *Proceedings of the Institution of Civil Engineers-Structures and Buildings*, *170*(10), 722-734.

Karavasilis, T.L., Blakeborough, T., & Williams, M. S. (2011). Development of nonlinear analytical model and seismic analyses of a steel frame with self-centering devices and viscoelastic dampers. *Computers & Structures*, *89*(11-12), 1232-1240.

Lagoudas, D. (2008). *Shape Memory Alloys-Modeling and Engineering Applications*. Texas A&M University TX, Springer: USA.

Lee, C.H., Kim, J., Kim, D.H., Ryu, J., & Ju, Y.K. (2016). Numerical and experimental analysis of combined behavior of shear-type friction damper and non-uniform strip damper for multi-level seismic protection. *Engineering Structures*, *114*, 75-92.

Li, G.Q., Sun, Y.Z., Jiang, J., Sun, F.F., & Ji, C. (2019). Experimental study on two-level yielding buckling-restrained braces. *Journal of Constructional Steel Research*, *159*, 260-269.

Li, H., Qian, H., & Song, G. (2008). Experimental and analytical investigation on innovative hybrid shape memory alloys dampers for structural control. *Active and Passive Smart Structures and Integrated Systems*.

Marshall, J.D., & Charney, F.A. (2010). A hybrid passive control device for steel structures, I: Development and analysis. *Journal of Constructional Steel Research*, *66*(10), 1278-1286.

Mazzoni, S., McKenna, F., Scott, M., & Fenves, G. (2006). *OpenSees Command Language Manual*. Pacific Earthquake Engineering Research Center: Berkeley Edu.

Morais, J., de Morais, P.G., Santos, C., Costa, A.C., & Candeias, P. (2017). Shape memory alloy-based dampers for earthquake response mitigation. *Procedia Structural Integrity*, *5*, 705-712.

Ozbulut, O.E., & Hurlebaus, S. (2012). Application of a SMA-based hybrid control device to 20-story nonlinear benchmark building. *Earthquake Engineering & Structural Dynamics*, *41*(13), 1831-1843.

Qian, H., Li, H., & Song, G. (2016). Experimental investigations of the building structure with a superelastic shape memory alloy friction damper subject to seismic loads. *Smart Materials and Structures*, *25*(12).

Qian, H., Li, H., Song, G., & Guo, W. (2013). Recentering shape memory alloy passive damper for structural vibration control. *Mathematical Problems in Engineering*.

Qiu, C., & Zhu, S. (2017). Shake table test and numerical study of self?centering steel frame with SMA braces. *Earthquake Engineering & Structural Dynamics*, *46*(1), 117-137.

Rawlinson, T., & Marshal, J. (2012). Multi-phase passive control systems for performance-base design. *Proceedings of 15th World Conference on Earthquake Engineering*.

Rousta, A.M., & Zahrai, S.M. (2017). Cyclic testing of innovative two-level control system: Knee brace & vertical link in series in chevron braced steel frames. *Structural Engineering and Mechanics*, *64*(3), 301-310.

Song, G., Ma, N., & Li, H.N. (2006). Applications of shape memory alloys in civil structures. *Engineering Structures*, *28*(9), 1266-1274.

Soong, T., & Spencer, J.B. (2002). Supplemental energy dissipation: state-of-the-art and state-of-the-practice. *Engineering Structures*, *24*, 243-259.

Symans, M.D., Charney, F.A., Whittaker, A.S., Constantinou, M.C., Kircher, C.A., W., J.M., & Mcnamara, R.J. (2008). Energy dissipation systems for seismic applications: current practice and recent developments. *ASCE J. Struct. Eng.*, *134*(1), 3-21.

Wang, W., Tang, Y.C., & Xu, W.K. (2013). Experimental and FEA Studies of a new type SMA viscous damper. *Applied Mechanics and Materials*, *353*, 1815-1818.

Yamamoto, M., & Sone, T. (2014). Damping systems that are effective over a wide range of

displacement amplitudes using metallic yielding component and viscoelastic damper in series. *Earthquake Engineering & Structural Dynamics*, *43*(14), 2097-2114.

Yang, C.S., DesRoches, R., & Leon, R.T. (2010). Design and analysis of braced frames with shape memory alloy and energy-absorbing hybrid devices. *Engineering Structures*, *32*(2), 498-507.

Zahrai, S.M., & Golmoghany, M.Z. (2021). Seismic behavior of a two-level control system with double vertical shear links in series. *Smart Structures and Systems, An International Journal*, *27*(3), 467-478.